

## ORIGINAL ARTICLE

# A visible light-driven plasmonic photocatalyst

Francesca Pincella<sup>1,2</sup>, Katsuhiro Isozaki<sup>1,3</sup> and Kazushi Miki<sup>1,2</sup>

We demonstrate a bottom-up approach to fabricating a visible light-driven titania photocatalyst device bearing an embedded two-dimensional (2D) array of gold nanoparticles (AuNPs) as a near-field light-generating layer. The device is a layered structure prepared by depositing a 2D array of AuNPs on a transparent conductive substrate (10 nm indium tin oxide (ITO) layer on quartz), coating the 2D array of AuNPs with a monolayer of trimethoxyoctylsilane (TMOS), and depositing titania nanocrystals on the anchoring molecule (TMOS) layer. The visible light activity of the device was tested using photocatalytic degradation of methylene blue (MB) by illuminating the device with visible light (700 nm light) and ultraviolet (UV) light (250–380 nm). The localized surface plasmon resonance peak of the 36 nm AuNP 2D array is around 700 nm with a full-width at half-maximum of 350 nm. In comparison with other control samples, the device showed the highest photocatalytic activity with visible irradiation, which was 1.7 times higher than that of titania with UV irradiation. The origin of the visible light activity was confirmed by both quadratic incident light power dependency and action spectrum to be plasmon-induced (near-field enhancement by AuNPs) two-photon absorption.

*Light: Science & Applications* (2014) 3, e133; doi:10.1038/lsa.2014.14; published online 17 January 2014

**Keywords:** gold nanoparticles; near-field light; plasmonics; two-photon absorption; visible photocatalysis

## INTRODUCTION

Since the discovery in 1968 of photocatalytic water splitting by Honda and Fujishima,<sup>1</sup> titania has been intensively studied for its photocatalytic properties,<sup>2,3</sup> which could be used to convert solar energy to storable chemical energy by hydrogen production,<sup>4</sup> or to address environmental issues such as the treatment of waste water<sup>5</sup> and cleaning of exterior windows<sup>6,7</sup> by degradation of organic molecules. The bandgap of titania allows the creation of an electron–hole (e–h) pair only when irradiated by ultraviolet (UV) light, which is just a small fraction (less than 5%) of the solar spectrum and this limits its usefulness as a solar photocatalyst. Many different approaches to overcome the limitations of titania have been proposed, notably doping of oxide semiconductors<sup>8</sup> or photosensitization of titania.<sup>9</sup> The doping of titania, despite the most common approach to decreasing the wide bandgap of the oxide semiconductor,<sup>10</sup> has many disadvantages. For example, the introduction of impurities strongly affects the lifetime of the e–h pair (impurities act as recombination centers), and doping can also decrease the corrosion resistance of the material (especially in the case of doping with transition metal ions).<sup>11</sup> Photosensitization of titania with organic dyes still presents major limitations for applications in photocatalysis due to the poor stability of the dye, which can undergo desorption, photolysis and oxidative degradation,<sup>12,13</sup> and fast back electron transfer, which results in low quantum yield for the photocatalytic reaction.<sup>14</sup> As an alternative to organic dyes, recently metallic nanostructures have been successfully used as photosensitizers

for wide bandgap semiconductors<sup>15–19</sup> thanks to their broad and strong visible absorption based on localized surface plasmon resonance (LSPR) and their excellent chemical stability. Efforts to date to produce metallic nanostructure sensitizers for wide bandgap semiconductors have focused on the development of plasmonic nanostructures that either allow fine control of the geometry (shape, size, interparticle gap distance) of the nanostructures with good reproducibility but small area, e.g., top-down techniques such as lithography,<sup>20</sup> or large-scale deposition with poor control of optical properties (LSPR wavelength and its width), e.g., self-assembly-based bottom-up techniques such as vapor deposition of island films<sup>21,22</sup> and the Langmuir–Blodgett method.<sup>23</sup> However, there has not been a good method of producing metallic nanostructure sensitizers for wide bandgap semiconductors with the advantages of large area, high density, fine tunable structure, mechanical durability and low cost. Our group recently developed a hybrid deposition method that overcomes the common limitations listed above; the method enables metal nanoparticle (MNP) two-dimensional (2D) arrays to be deposited over large substrates with high mechanical durability and high MNP coverage.<sup>24–26</sup> Under resonant conditions (light excites LSPR in the MNPs), the 2D array generates strong near-field (NF) light in the proximity of the MNPs ('hot spots'<sup>27,28</sup>), which was shown to be able to induce two-photon absorption (TPA) in a fluorescent dye deposited on gold nanoparticles (AuNPs).<sup>24</sup> Our method of producing dense large-area 2D arrays of MNPs is thus expected to act as a powerful sensitizer for wide bandgap

<sup>1</sup>Polymer Materials Unit, National Institute for Materials Science, Ibaraki 305-0044, Japan; <sup>2</sup>Department of Pure and Applied Sciences, University of Tsukuba, Ibaraki 305-8571, Japan; <sup>3</sup>Current address: International Research Center for Elements Science, Institute for Chemical Research, Kyoto University, Kyoto 611-0011, Japan

Correspondence: Dr K Isozaki, International Research Center for Elements Science, Institute for Chemical Research, Kyoto University, Gokasyo, Uji, Kyoto 611-0011, Japan  
E-mail: kisozaki@scl.kyoto-u.ac.jp

Or Professor KM, Polymer Materials Unit, National Institute for Materials Science, 1-1 Namiki, Tsukuba, Ibaraki 305-0044, Japan

E-mail: MIKI.Kazushi@nims.go.jp

Received 16 June 2013; revised 5 September 2013; accepted 21 September 2013

semiconductors. Here, we report the development of a self-assembly-based bottom-up, large-scale, cheap (no clean room facilities or high temperature are needed) and reproducible photocatalytic device whose optical properties can be controlled by fine LSPR tuning *via* MNP size and interparticle distance.<sup>24–26</sup>

## MATERIALS AND METHODS

### General

Ultraviolet–visible (UV–Vis) extinction spectra were recorded with a Jasco V-670, and scanning electron microscope (SEM) images were acquired with a Hitachi S-4800 FE-SEM. Raman measurements were performed with a Horiba Jobin-Yvon T-64000 microRaman spectrometer equipped with an Ar<sup>+</sup>/Kr<sup>+</sup> laser (514.5 nm excitation line was used). An Asahi-Spectra 300 W Xe lamp (Max-302) equipped with UV (250–385 nm), Vis (385–740 nm) and IR (750–1050 nm) mirrors and different bandpass filters was used for the photocatalytic degradation experiments. Small-angle X-ray scattering (SAXS) measurements were performed using beamline BL40B2 with synchrotron radiation at SPring-8 (Hyogo, Japan). X-ray diffraction patterns were obtained with a RIGAKU RINT2000 Ultima-III. Transmission electron microscope (TEM) images were obtained with a JEOL JEM 2100-F, and contact angle measurements were performed with a Kyowa DM500 contact angle meter. Atomic force microscope (AFM) images were acquired with a SII NanoTechnology L-Trace AFM in tapping mode with a Si cantilever.

### Materials

Plastic-formed carbon counter electrodes were purchased from Tsukuba Materials Information Laboratory Ltd and used after cutting and cleaning by sonication in deionized water and hexane. All reagents were purchased from Sigma-Aldrich Co. (Tokyo, Japan), Tokyo Chemical Industry Co., Ltd (Kyoto, Japan) and Nacalai Tesque, Inc.

### Substrate preparation

Quartz substrates (1 cm×1 cm) were cleaned by immersion for 15 min at room temperature in fresh piranha solution (30% H<sub>2</sub>SO<sub>4</sub>/H<sub>2</sub>O<sub>2</sub> = 2 : 1 v/v; handle with care: piranha solution is highly corrosive and reacts violently with organic matter) and rinsing three times with milli-Q water. The substrates were then coated with indium tin oxide (ITO) (10 nm) by radiofrequency sputtering deposition at room temperature, followed by UV-ozone cleaning for 3 h (final bulk resistivity of 1.1 × 10<sup>−3</sup> Ω cm). The substrates were immersed in a 1% (v/v) solution of 3-mercaptopropyltrimethoxysilane in toluene for 40 h, rinsed with methanol three times and dried with a nitrogen stream. Finally, the substrates were immersed in a 1% (v/v) solution of 1,6-hexanedithiol in ethanol for 12 h, rinsed with acetone three times and dried with a nitrogen stream.

### Synthesis of gold nanoparticles

Gold nanoparticles (AuNPs) were synthesized by the citrate reduction method (average size 36 ± 6 nm);<sup>29</sup> a 100 mL solution of 0.5 mM HAuCl<sub>4</sub>·3H<sub>2</sub>O was brought to boiling in a round bottom flask while continuously stirring, then 2.2 mL of a 38.8 mM aqueous sodium citrate solution were added at once. The solution was refluxed for 20 min to allow complete reduction (solution turned wine red). The extinction spectrum of the colloidal solution of AuNPs is shown in Supplementary Fig. S1.

The 36 nm AuNPs were then capped with mixed alkanethiols;<sup>24</sup> 10 mL of colloidal solution of gold nanoparticles were mixed with a 0.28% (v/v) mixed alkanethiols (hexanethiol/dodecanethiol = 3 : 1) solution in 10 mL of acetone. Stirring was performed for 1 h, then alkanethiol-capped AuNPs were extracted with acetone and hexane

and purified by sequential centrifuge and redispersion into hexane three times.

### Synthesis of titania nanocrystals

Titania nanocrystals solution was prepared by the controlled hydrolysis of tetraisopropyl titanate as described in the literature,<sup>30</sup> and the concentration was adjusted to 10 mg mL<sup>−1</sup> in ethanol–water (2 : 1, v/v) by rotary evaporation. The average size of the titania nanocrystals (3.5 nm) was determined from TEM images and confirmed from the X-ray diffraction pattern (3 nm from the Debye–Scherrer equation) and Raman spectrum<sup>31</sup> (below 4 nm as determined from full-width at half-maximum of the *E<sub>G</sub>* (Equation (1)) phonon peak) (Supplementary Fig. S2). The titania nanocrystals were proven to be mainly in the anatase form, as shown in the X-ray diffraction pattern (only trace of rutile) and Raman spectrum (no rutile contribution was detected from the Raman spectrum) (Supplementary Fig. S2). The bandgap of a thin film of titania nanocrystals was determined from the equation:<sup>32</sup>

$$\alpha = B_i(h\nu - E_G)^{1/2}/h\nu \quad (1)$$

where *B<sub>i</sub>* is the absorption coefficient for direct transition,  $\alpha$  is the absorbance and *E<sub>G</sub>* is the bandgap energy of the semiconductor. From the linear fit of  $(\alpha h\nu)^2$  versus *hν*, the value for the bandgap energy was obtained as 3.34 eV (Supplementary Fig. S2b). The titania nanocrystals showed a direct transition instead of an indirect transition and an energy gap larger than expected for bulk anatase titania (3.2 eV) in agreement with previously reported results<sup>32</sup> for nanosized titania samples.

### Deposition of titania layer

The effectiveness of trimethoxyoctylsilane (TMOS) as an anchoring agent was verified by preparing two identical 2D arrays of AuNPs: one of them was coated with TMOS prior to immersion in titania solution, while the other was directly immersed in titania solution without anchoring molecules. Both samples were sonicated repeatedly to test the mechanical durability of titania. As a result, the sample without TMOS presented a clear change in the extinction spectrum with increasing sonication time, while the sample protected with the TMOS layer exhibited only a minor change, as shown in Supplementary Fig. S3.

The effectiveness of titania nanocrystals deposition was determined by contact angle measurements, comparing the contact angle before and after titania deposition. A change from hydrophobic to hydrophilic surface was observed (Supplementary Fig. S4), in good agreement with the reported hydrophilicity of titania.<sup>33</sup>

After titania deposition, the sample was also characterized with SEM and AFM (Supplementary Fig. S5), as well as SAXS (performed at SPring-8, beamline BL40B2; Supplementary Fig. S6), to evaluate the effect of titania deposition on sample morphology and 2D array structure. The SEM and AFM images revealed that titania was deposited on the array, preferably in the space near the gap between AuNPs, even though the titania layer was inhomogeneous, while the SAXS patterns indicated that the 2D array structure was retained, since only a small shift in the peak position was observed (corresponding to a shift in the interparticle distance of about 0.8 nm comparing the SAXS pattern before and after TMOS and titania deposition).

## RESULTS AND DISCUSSION

We planned to exploit the strong NF light induced by a 2D array of AuNPs to enable visible light activity in titania nanocrystals deposited on the top of the array. The device was prepared as follows: a 2D array of AuNPs was deposited on a transparent conductive substrate (10 nm

ITO on quartz), then an anchoring molecule (TMOS) was arranged on the array to enable strong attachment between AuNPs and the titania nanocrystals, as shown in Figure 1.

AuNPs were synthesized by the citrate reduction method (average size:  $36 \pm 6$  nm).<sup>29</sup> The 36 nm AuNPs were then capped with mixed alkanethiols<sup>24</sup> (hexanethiols/dodecanethiols = 3 : 1). The AuNPs were then arrayed on a thiol-terminated ITO/quartz substrate by means of our hybrid deposition method,<sup>24</sup> which uses electrophoretic deposition, solvent evaporation and self-assembly to form a monolayer which is strongly bound to the substrate. Briefly, AuNPs were redispersed in 6 mL of hexane–acetone (3 : 1, *v/v*) and added to an open vessel where a voltage (1.1 V) was applied between the thiol-terminated ITO substrate (cathode) and plastic carbon (anode) electrodes placed 1.2 mm apart from each other. After solvent evaporation was completed, the sample was annealed at 50 °C for 12 h to enable chemisorption (Au–S bond) of AuNPs on the functionalized ITO substrates. Finally, the sample was sonicated in hexane for 30 s to remove multilayers. The AuNP coverage exceeded 90% over the whole substrate area (1 cm × 1 cm) as shown in Figure 2a.

The surface of the 2D array was further functionalized by TMOS to result in siloxane termination, taking advantage of the intermolecular hydrophobic interaction between alkyl chains.<sup>25</sup> The 2D array of AuNPs was coated with a monolayer of TMOS by dropping 20  $\mu$ L of a 1% (*v/v*) solution of TMOS in MeOH onto the 2D array. The sample was kept in a MeOH vapor-saturated environment for 1 h, rinsed with MeOH and dried with a nitrogen stream. The anchoring molecule will both induce strong mechanical durability of the titania layer (Supplementary Fig. S3) and act as a thin dielectric layer to partially inhibit charge transfer between AuNPs and TiO<sub>2</sub>. Small titania nanocrystals<sup>30</sup> (mean diameter of approx. 3.5 nm, anatase phase with trace rutile, see Figure 2 and Supplementary Fig. S2) were chosen to allow fast migration of the e–h pair at the surface and also to fully take advantage of the NF light in the proximity of the gap between AuNPs. Titania deposition was performed by immersing the sample in a solution of titania nanocrystals in ethanol–water overnight at 37 °C, rinsing the sample with water and annealing at 90 °C for 12 h. The

titania-coated 2D array was then characterized by UV-Vis-NIR spectroscopy, SEM, AFM and SAXS to verify the effective deposition of the titania nanocrystals (Figure 2c and Supplementary Figs. S4, S5 and S6). The average thickness (7.6 nm) of the titania layer on the array corresponds to about two layers of nanocrystals, as confirmed from TEM cross-sectional images (Figure 2b). As these results indicate, this device takes full advantage of a chemical bottom-up approach since each solid layer is strongly attached by molecular building blocks whose mutual interactions contribute to the construction of a complex multilayered device: dithiols self-organize on the ITO surface, metallic nanoparticles are immobilized on the substrate due to Au–S bonds, TMOS is attached to the metallic particles *via* hydrophobic interaction, and titania is immobilized through Ti–O–Si covalent bonds.<sup>34</sup>

In order to test the visible light activity of our device, photocatalytic degradation of methylene blue (MB) was performed by illuminating our device and the control samples with visible light (700 nm light) and UV light (250–380 nm). Irradiation with 700 nm light was chosen in order to excite the LSPR of the 2D array, while concurrently minimizing the direct excitation of MB; UV irradiation was used to verify the photodegradation activity of the array when TiO<sub>2</sub> was excited directly (photon energy is sufficient to induce e–h pair creation). Control samples, namely bare quartz, a 2D array of AuNPs and quartz coated with titania nanocrystals (for further details about the preparation of control samples, see Supplementary Information), were prepared in order to rule out different pathways for organic dye photodegradation, such as self-sensitization,<sup>9,35</sup> direct photolysis<sup>36</sup> and degradation by LSPR heating.<sup>37</sup> Samples for photocatalytic degradation of MB were prepared by drop-casting 40  $\mu$ L of 65  $\mu$ M solution of MB in MeOH on the samples (at 90 °C) giving a dye density of about 16 nmol cm<sup>–2</sup>. Each sample was irradiated with a 300 W Xe lamp (MAX-302; Asahi Spectra Co., Ltd (Tokyo, Japan)) equipped with UV (250–385 nm), Vis (385–740 nm) and IR (750–1050 nm) mirrors and different bandpass filters (700 nm with 10 nm full-width at half-maximum filter). MB photodegradation was performed in air since oxygen in air acts as an electron scavenger, having the multiple effects of

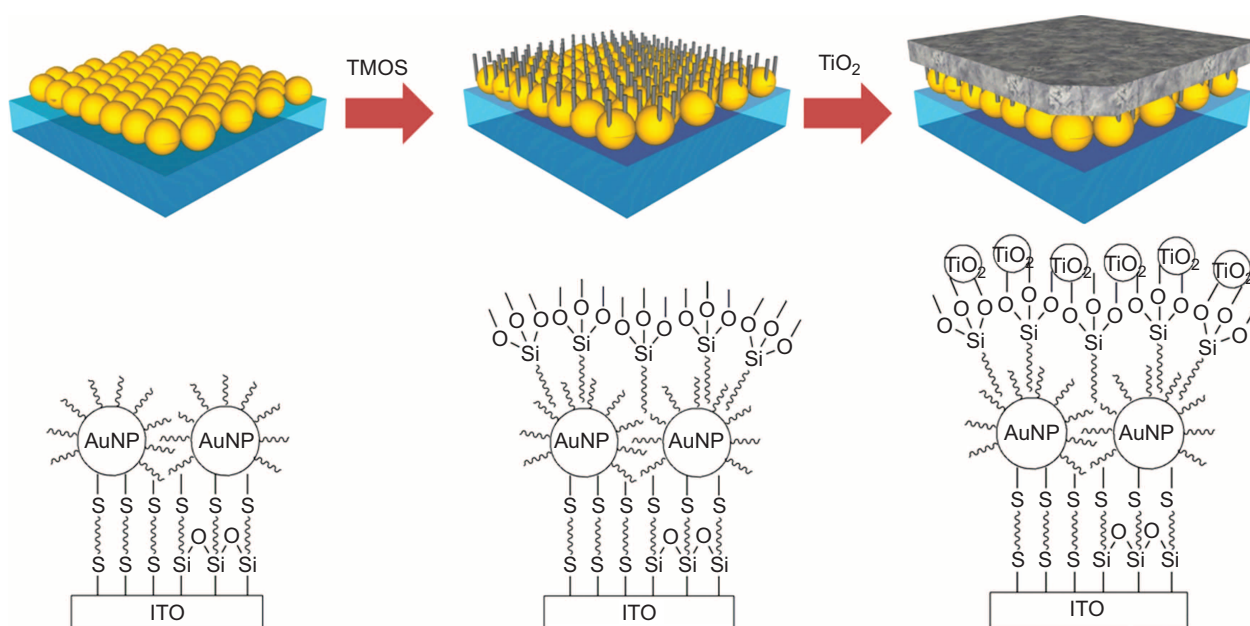


**Figure 1** Schematic illustration of process of preparing the proposed plasmonic photocatalyst.



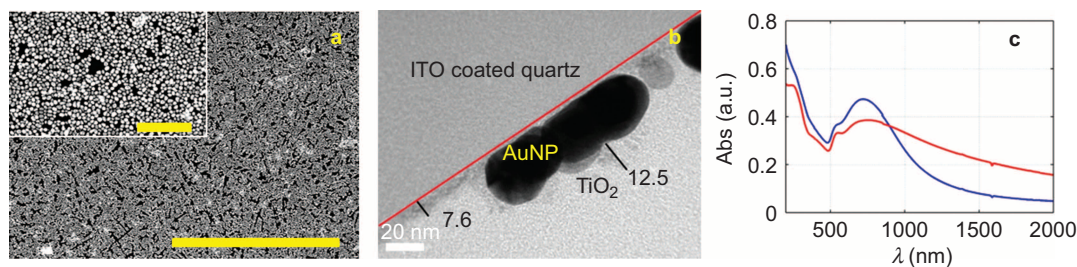


**Figure 2** (a) SEM image of the 2D array of 36 nm AuNPs (scale bar = 5 μm). Inset: high magnification (scale bar = 500 nm). (b) TEM cross-sectional image of the titania-coated 2D array. The two black lines indicate the titania layer thickness in nm, the red line indicates the top of the ITO layer. (c) Extinction spectra of 2D array before (blue line) and after titania coating and annealing (red line). 2D, two-dimensional; ITO, indium tin oxide; SEM, scanning electron microscope; TEM, transmission electron microscope.

inhibiting fast recombination of the e-h pair, avoiding the reduction of MB to leucomethylene blue, and providing reactive oxygen species that contribute to MB photodegradation.<sup>38</sup>

In order to evaluate the photocatalytic activity of all samples, the extinction spectrum was checked at regular intervals and the degradation rate was evaluated from the peak intensity decrease *versus* irradiation time (Supplementary Fig. S7). For each value of MB peak intensity, we waited for 15 min prior to acquisition of the UV-Vis spectrum to ensure equilibrium (three UV-Vis spectra were collected after irradiation at 5 min intervals to verify the relaxation to equilibrium). Initial reaction steps of all samples showed pseudo first-order kinetics; thus, each photocatalytic degradation rate *k* was obtained from the linear fit of:

$$\ln(I/I_0) = -kt \quad (2)$$

The values of photocatalytic activity are shown as MB degradation rate divided by incident power for all samples (device and control samples) and for both visible (700 and 10 nm full-width at half-maximum) and UV irradiation (250–385 nm). The maximum photocatalytic activity was achieved with the titania-coated 2D array excited with visible light as expected. Note that the value of photocatalytic activity of the titania-coated 2D array exceeds the photocatalytic activity of the titania nanocrystal-coated ITO sample irradiated with UV light by 1.7 times. In addition, the photocatalytic activity of the titania-coated 2D array irradiated with visible light was 14 times higher than that irradiated with UV light; the low photocatalytic activity of the layered device under UV irradiation is probably due to the previously proposed<sup>15</sup> charge depletion (Schottky barrier at the titania/Au interface) from titania to AuNPs and to the high extinction of Au in the UV region. By evaluating the photocatalytic degradation rate for the titania sample irradiated with visible light in Figure 3, we could exclude major contributions from the direct visible light activity of titania (the bandgap of titania nanocrystals was calculated from the UV-Vis extinction spectrum to be 3.34 eV, see Supplementary Fig. S2b) and self-sensitization, which consist of excitation of dye by visible light, consequent transfer of energy from the dye (typical mechanism of dye-sensitized cells) to the oxide semiconductor which then undergoes e-h pair creation, and finally charge transfer to the dye, inducing photocatalytic degradation. The low degradation rate for the MB-coated quartz substrate also indicated that direct photolysis was not the main contributor to the visible light activity of the device. Lastly, by comparing the photocatalytic degradation rate of the titania-coated array and the uncoated 2D array, we excluded the possibility that the LSPR effect by itself (plasmonic heat<sup>39</sup> or energy transfer<sup>40</sup>) is responsible for visible light photocatalytic degradation, that is, excitation of MNPs alone

is not able to induce a noticeable modification of MB. In conclusion, we proved that the combination of MNPs 2D array and titania layer is indispensable for obtaining visible-light induced photocatalytic activity.

Once different reaction pathways were excluded, we could investigate the origin of the visible light activity of titania. To do this, we checked the dependence of photocatalytic degradation rate on excitation wavelength (Supplementary Fig. S8) and found that the maximum rate corresponded with the peak value of LSPR, and that the tendency of the rate was similar to the shape of the LSPR peak,

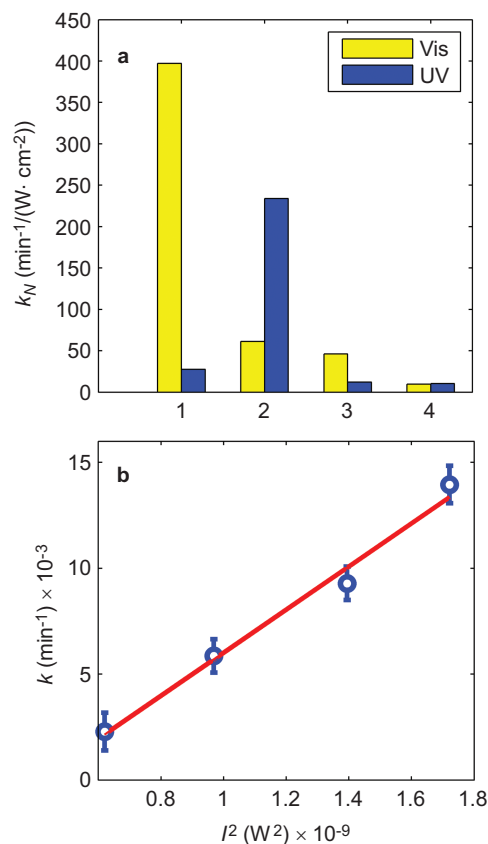


**Figure 3** (a) Histogram showing the normalized photocatalytic degradation rate calculated from the initial photocatalytic degradation rate for various samples. Values on the x axis correspond to four different samples coated with MB to perform the photocatalytic degradation experiment. The samples are: (1) titania-coated 2D array, (2) titania-coated ITO substrate, (3) 2D array and (4) bare quartz substrate. (b) Linear fitting of photocatalytic degradation rate *versus* second power of the incident light. 2D, two-dimensional; ITO, indium tin oxide; MB, methylene blue.

suggesting plasmon-induced visible light activity. In fact, this tendency is in agreement with a well-known property of MNPs (this property is valid for small spherical MNPs for which the far-field and near-field resonant frequencies overlap completely),<sup>41</sup> namely, that the highest near-field enhancement can be achieved when light is resonant with the MNPs' LSPR (wavelength of the excitation light corresponds to the LSPR peak of the MNPs' UV-Vis spectrum).

Plasmon-induced visible light activity can originate from different interactions of MNPs with titania; therefore, further analysis is needed. Direct plasmonic excitation can be partially ruled out, namely, direct enhancement of visible light activity, due to the large bandgap of titania nanocrystals, allowing excitation only by UV light and LSPR of the 2D array, which instead lies in the NIR region of 755 nm (Figure 2c). A second direct mechanism, 'hot electron' transfer, is also partially inhibited owing to the TMOS layer deposited on the AuNPs. Excluding these two mechanisms and considering that the LSPR wavelength of our plasmonic device (755 nm) corresponds to about twice the wavelength relative to the titania bandgap (371 nm), TPA was assumed to be the main contributor to the visible light activity of titania (excitation resonant with the LSPR is able to induce the formation of e-h pairs in titania due to simultaneous absorption of two photons<sup>20,42</sup>). To verify this assumption, we performed MB photocatalytic degradation with 700 nm light while varying the incident power with a neutral density filter. It is well known that the power dependence of titania photocatalytic reactions is affected by the titania thickness; in the case of the bulk state, only the region near the surface of titania would contribute to photocatalytic reactions owing to the short lifetime of the photocarriers and the power dependence would follow a root-square power law.<sup>43</sup> In the case of nanosized titania, a linear power dependence was verified since all photogenerated charges can migrate at the interface and contribute to the reaction. In our experiment, the small size of titania nanocrystals (3.5 nm) would suggest a linear behavior in the case of linear absorption. However, the experimental results shown in Figure 3b indicate a square power dependence, which clearly shows that the photocatalytic degradation of MB is induced by TPA with embedded AuNP arrays.

Finally, we investigated the photocatalytic activity of our device under wide band visible light illumination (Xe lamp with 422–750 nm filter). The result of visible light irradiation confirmed the higher photocatalytic activity (6.5 times higher) of our sample compared to the titania reference sample, as shown in Figure 4. This result

shows that visible light is suitable for the excitation of wide LSPR absorption of 2D arrays of AuNPs.

In addition, solar light irradiation was tested and the result (the photocatalytic activity of our device was twice that of the titania reference; see Supplementary Fig. S9) showed the potential of our photocatalytic device for converting solar energy to chemical energy.

## CONCLUSION

In summary, a visible light photocatalytic device was fabricated by means of only wet chemical bottom-up deposition processes, without needing expensive clean-room deposition processes or high-temperature treatments. The photocatalytic activity of the device was investigated by photocatalytic degradation of MB with visible and UV irradiation. In comparison with other control samples, our device showed the highest photocatalytic activity with visible irradiation, which was 1.7 times higher than that of titania with UV irradiation. The origin of such visible light activity was confirmed to be TPA by both quadratic incident light power dependency and action spectrum. TPA was proven to be induced by the strong NF light originating in the proximity of AuNPs when localized surface plasmons were excited ( $\lambda_{\text{ex}} \approx \lambda_{\text{LSPR}}$ ). The result of MB photocatalytic degradation with a titania-coated 2D array under wide band visible light irradiation is encouraging, since the photocatalytic degradation rate for a titania-coated 2D array is more than six times that of the titania sample.

## ACKNOWLEDGMENTS

We thank the Japan Society for the Promotion of Science and the Ministry of Education, Culture, Sports, Science and Technology of Japan for financial support; Grant-in-Aid for Challenging Exploratory Research (KM, 24656040); Grant-in-Aid for Scientific Research on Innovative Areas 'Integrated Organic Synthesis' (KM, 22106545 and 24106746); and Grant-in-Aid for Young Scientists (KI, 30455274), Japan Science and Technology Agency for financial support of e-ASIA JRP. Also, a part of this research was supported by the Research Foundation for Opto-Science and Technology, by Grant for Environmental Research Projects from The Sumitomo Foundation and the Collaborative Research Program of the Institute for Chemical Research, Kyoto University (grant 2012-14). We are grateful to Professor M Nakamura and Professor H Takaya (Kyoto University) for their assistance with the analysis and helpful discussions. SAXS measurements were performed at BL40B2, SPring-8, with the approval of the Japan Synchrotron Radiation Research Institute (Grant No. 2010B1744, 2012A1575).

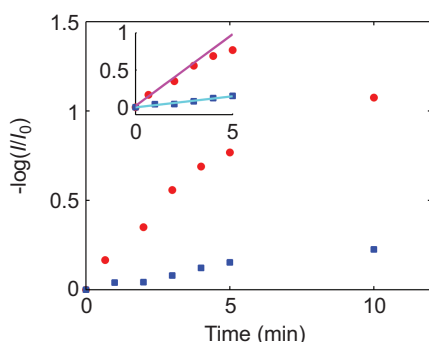


**Figure 4** MB photocatalytic degradation under wide band visible light illumination. The photocatalytic degradation experiment was performed with titania-coated 2D array (red circles) and titania-coated ITO substrate (blue squares). Inset: pseudo first-order kinetics of initial reaction steps for titania-coated 2D array and titania sample. 2D, two-dimensional; ITO, indium tin oxide; MB, methylene blue.

- 1 Fujishima A, Honda K. Electrochemical photolysis of water at a semiconductor electrode. *Nature* 1972; **238**: 37–38.
- 2 Ni M, Leung MK, Leung DY, Sumathy K. A review and recent developments in photocatalytic water-splitting using TiO<sub>2</sub> for hydrogen production. *Renew Sustain Energy Rev* 2007; **11**: 401–425.
- 3 Kumar SG, Devi LG. Review on modified TiO<sub>2</sub> photocatalysis under UV/visible light: selected results and related mechanisms on interfacial charge carrier transfer dynamics. *J Phys Chem A* 2011; **115**: 13211–13241.
- 4 Szymanski P, El-Sayed M. Some recent developments in photoelectrochemical water splitting using nanostructured TiO<sub>2</sub>: a short review. *Theor Chem Acc* 2012; **131**: 1–12.
- 5 Lachheb H, Puzenat E, Houas A, Ksibi M, Elaloui E *et al*. Photocatalytic degradation of various types of dyes (Alizarin S, Crocein Orange G, Methyl Red, Congo Red, Methylene Blue) in water by UV-irradiated titania. *Appl Catal B* 2002; **39**: 75–90.
- 6 Rampaul A. Titania and tungsten doped titania thin films on glass; active photocatalysts. *Polyhedron* 2003; **22**: 35–44.
- 7 Paz Y, Luo Z, Rabenberg L, Heller A. Photooxidative self-cleaning transparent titanium dioxide films on glass. *J Mater Res* 1995; **10**: 2842–2848.
- 8 Khan SU, Al-Shahry M, Ingler WB. Efficient photochemical water splitting by a chemically modified n-TiO<sub>2</sub>. *Science* 2002; **297**: 2243–2245.
- 9 Zhao J, Chen C, Ma W. Photocatalytic degradation of organic pollutants under visible light irradiation. *Top Catal* 2005; **35**: 269–278.
- 10 Leung DY, Fu X, Wang C, Ni M, Leung MK *et al*. Hydrogen production over titania-based photocatalysts. *Chem Sus Chem* 2010; **3**: 681–694.

- 11 Kisch H, Macyk W. Visible-light photocatalysis by modified titania. *Chem Phys Chem* 2002; **3**: 399–400.
- 12 Bard A, Fox M. Artificial photosynthesis: solar splitting of water to hydrogen and oxygen. *Acc Chem Res* 1995; **28**: 141–145.
- 13 Wu T, Liu G, Zhao J. Photoassisted degradation of dye pollutants. V. Self-photosensitized oxidative transformation of rhodamine B under visible light irradiation in aqueous TiO<sub>2</sub> dispersions. *J Phys Chem B* 1998; **102**: 5845–5851.
- 14 Zhao Y, Swierk JR, Megiatto JD, Sherman B, Youngblood WJ *et al*. Improving the efficiency of water splitting in dye-sensitized solar cells by using a biomimetic electron transfer mediator. *Proc Natl Acad Sci USA* 2012; **109**: 15612–15616.
- 15 Mubeen S, Hernandez-Sosa G, Moses D, Lee J, Moskovits M. Plasmonic photosensitization of a wide band gap semiconductor: converting plasmons to charge carriers. *Nano Lett* 2011; **11**: 5548–5552.
- 16 Wang X, Blackford M, Prince K, Caruso RA. Preparation of boron-doped porous titania networks containing gold nanoparticles with enhanced visible-light photocatalytic activity. *ACS Appl Mater Interface* 2012; **4**: 476–482.
- 17 Primo A, Corma A, García H. Titania supported gold nanoparticles as photocatalyst. *Phys Chem Chem Phys* 2011; **13**: 886–910.
- 18 Liu Z, Hou W, Pavaskar P, Aykol M, Cronin S. Plasmon resonant enhancement of photocatalytic water splitting under visible illumination. *Nano Lett* 2011; **11**: 1111–1116.
- 19 Christopher P, Ingram DB, Linic S. Enhancing photochemical activity of semiconductor nanoparticles with optically active Ag nanostructures: photochemistry mediated by Ag surface plasmons. *J Phys Chem C* 2010; **114**: 9173–9177.
- 20 Ueno K, Juodkazis S, Shibuya T, Yokota Y, Mizeikis V *et al*. Nanoparticle plasmon-assisted two-photon polymerization induced by incoherent excitation source. *J Am Chem Soc* 2008; **130**: 6928–6929.
- 21 Schlegel VL, Cotton TM. Silver-island films as substrates for enhanced Raman scattering: effect of deposition rate on intensity. *Anal Chem* 1991; **63**: 241–247.
- 22 Desiredy A, Joshi CP, Sestak M, Little S, Kumar S *et al*. Wafer-scale self-assembled plasmonic thin films. *Thin Solid Films* 2011; **519**: 6077–6084.
- 23 Huang S, Tsutsui G, Sakaue H, Shingubara S, Takahagi T. Experimental conditions for a highly ordered monolayer of gold nanoparticles fabricated by the Langmuir–Blodgett method. *J Vac Sci Technol B* 2001; **19**: 2045.
- 24 Isozaki K, Ochiai T, Taguchi T, Nittoh K, Miki K. Chemical coating of large-area Au nanoparticle two-dimensional arrays as plasmon-resonant optics. *Appl Phys Lett* 2010; **97**: 221101.
- 25 Taguchi T, Isozaki K, Miki K. Enhanced catalytic activity of self-assembled-monolayer-capped gold nanoparticles. *Adv Mater* 2012; **24**: 6462–6467.
- 26 Ochiai T, Isozaki K, Pincella F, Taguchi T, Nittoh K *et al*. Plasmon-resonant optics on an indium-tin-oxide film for exciting a two-photon photochromic reaction. *Appl Phys Express* 2013; **6**: 102001.
- 27 Moskovits M. Surface-enhanced spectroscopy. *Rev Mod Phys* 1985; **57**: 783–826.
- 28 Kneipp K, Kneipp H, Itzkan I, Dasari R, Feld M. Surface-enhanced Raman scattering and biophysics. *J Phys Condens Matter* 2002; **14**: R597.
- 29 Frens G. Controlled nucleation for the regulation of the particle size in monodisperse gold suspensions. *Nature* 1973; **241**: 20–22.
- 30 Choi W, Termin A, Hoffmann MR. The role of metal ion dopants in quantum-sized TiO<sub>2</sub>: correlation between photoreactivity and charge carrier recombination dynamics. *J Phys Chem* 1994; **98**: 13669–13679.
- 31 Swamy V, Kuznetsov A, Dubrovinsky L, Caruso R, Shchukin D *et al*. Finite-size and pressure effects on the Raman spectrum of nanocrystalline anatase TiO<sub>2</sub>. *Phys Rev B* 2005; **71**: 184302.
- 32 Serpone N, Lawless D, Khairutdinov R. Size effects on the photophysical properties of colloidal anatase TiO<sub>2</sub> particles: size quantization or direct transitions in this indirect semiconductor? *J Phys Chem* 1995; **99**: 16646–16654.
- 33 Wang XP, Yu Y, Hu XF, Gao L. Hydrophobicity of TiO<sub>2</sub> films prepared by liquid phase deposition. *Thin Solid Films* 2000; **371**: 148–152.
- 34 Niesen TP, Bill J, Aldinger F. Deposition of titania thin films by a peroxide route on different functionalized organic self-assembled monolayers. *Chem Mater* 2001; **13**: 1552–1559.
- 35 Chatterjee D, Mahata A. Visible light induced photodegradation of organic pollutants on dye adsorbed TiO<sub>2</sub> surface. *J Photochem Photobiol A* 2002; **153**: 199–204.
- 36 Tang J, Zou Z, Yin J, Ye J. Photocatalytic degradation of methylene blue on CaIn<sub>2</sub>O<sub>4</sub> under visible irradiation. *Chem Phys Lett* 2003; **382**: 175–179.
- 37 Alessandri I, Depero LE. Using plasmonic heating of gold nanoparticles to generate local SER(R)S-active TiO<sub>2</sub> spots. *Chem Commun* 2009; (17): 2359–2361.
- 38 Tatsuma T, Tachibana S, Miwa T. Remote bleaching of methylene blue by UV-irradiated TiO<sub>2</sub> in the gas phase. *J Phys Chem B* 1999; **103**: 18–20.
- 39 Tong L, Wei Q, Wei A, Cheng J. Gold nanorods as contrast agents for biological imaging: optical properties, surface conjugation and photothermal effects. *Photochem Photobiol* 2009; **85**: 21–32.
- 40 Eichelbaum M, Rademann K. Plasmonic enhancement or energy transfer? On the luminescence of gold-, silver-, and lanthanide-doped silicate glasses and its potential for light-emitting devices. *Adv Funct Mater* 2009; **19**: 2045–2052.
- 41 Bryant GW, García de Abajo FJ, Aizpurua J. Mapping the plasmon resonances of metallic nanoantennas. *Nano Lett* 2008; **8**: 631–636.
- 42 Wu B, Ueno K, Yokota Y, Sun K, Zeng H *et al*. Enhancement of a two-photon-induced reaction in solution using light-harvesting gold nanodimer structures. *J Phys Chem Lett* 2012; **3**: 1443–1447.
- 43 Linic S, Christopher P, Ingram DB. Plasmonic-metal nanostructures for efficient conversion of solar to chemical energy. *Nat Mater* 2011; **10**: 911–921.



This work is licensed under a Creative Commons Attribution 3.0 Unported license. To view a copy of this license, visit <http://creativecommons.org/licenses/by/3.0>

Supplementary information for this article can be found on the *Light: Science & Applications* website (<http://www.nature.com/lsa/>).